

Article

Ericaria amentacea Algae Extracts: A Sustainable Approach for the Green Synthesis of Silver Oxide Nanoparticles and Their Effectiveness against Leishmaniasis

Fatouma Mohamed Abdoul-Latif ^{1,*}, Ayoub Ainane ², Ibrahim Houmed Aboubaker ³,
Barwako Houssein Kidar ⁴, Jalludin Mohamed ¹, Meryem Lemrani ⁵, Abdelmjid Abourriche ⁶
and Tarik Ainane ²

- ¹ Medicinal Research Institute, Center for Studies and Research of Djibouti, IRM-CERD, Route de l'Aéroport, Haramous, Djibouti City P.O. Box 486, Djibouti; mohamed.jalludin@gmail.com
 - ² Superior School of Technology of Khenifra (EST-Khenifra), University of Sultan Moulay Slimane, P.O. Box 170, Khenifra 54000, Morocco; a.ainane@usms.ma (A.A.); t.ainane@usms.ma (T.A.)
 - ³ Peltier Hospital of Djibouti, Djibouti City P.O. Box 2123, Djibouti; ibrahimhoumed@yahoo.fr
 - ⁴ Direction of the Blue, Green and Circular Economy, Industrial Zone, Commune of Boulaos, BP 11, Djibouti City P.O. Box 486, Djibouti; barwakohoussein@gmail.com
 - ⁵ Laboratory of Parasitology and Vector-Borne-Diseases, Institut Pasteur du Maroc, Casablanca 20360, Morocco; meryem.lemrani@pasteur.ma
 - ⁶ Laboratory of Analytical and Molecular Chemistry, Faculty of Sciences Ben M'sik, University of Hassan II, Casablanca 20700, Morocco; a.abourriche@gmail.com
- * Correspondence: fatoumaabdoulatif@gmail.com



Citation: Mohamed Abdoul-Latif, F.; Ainane, A.; Aboubaker, I.H.; Houssein Kidar, B.; Mohamed, J.; Lemrani, M.; Abourriche, A.; Ainane, T. *Ericaria amentacea* Algae Extracts: A Sustainable Approach for the Green Synthesis of Silver Oxide Nanoparticles and Their Effectiveness against Leishmaniasis. *Processes* **2023**, *11*, 3227. <https://doi.org/10.3390/pr11113227>

Academic Editors: Sechul Chun and Elwira Sieniawska

Received: 8 October 2023

Revised: 7 November 2023

Accepted: 13 November 2023

Published: 15 November 2023



Copyright: © 2023 by the authors. Licensee MDPI, Basel, Switzerland. This article is an open access article distributed under the terms and conditions of the Creative Commons Attribution (CC BY) license (<https://creativecommons.org/licenses/by/4.0/>).

Abstract: In this study, anti-leishmanial activities were performed on silver oxide nanoparticles green synthesized from hexane, ethereal, chloroform, and methanolic extracts of the *Ericaria amentacea* seaweed. The extracts were obtained using a Soxhlet extraction system, and the silver oxide nanoparticles were synthesized through a simple and environmentally friendly method. Physicochemical characterizations, including UV spectrophotometry, transmission electron microscopy (TEM), X-ray diffraction (XRD), thermal gravimetry analysis (TGA), Fourier-transform infrared spectroscopy (FTIR), and zeta potential analysis (ZPA), were conducted to confirm the formation of silver oxide particles. The anti-leishmanial activity was evaluated in vitro using the MTT assay against the *Leishmania infantum*, *Leishmania tropica*, and *Leishmania major* strains. Additionally, a brine shrimp cytotoxicity test was performed on *Artemia salina* larvae to assess the toxicity of the products. The results showed that the anti-leishmanial activity of the synthesized silver oxide nanoparticles was significant, with inhibitory concentration values ranging from 27.16 µg/mL to 38.18 µg/mL. The lethal doses in the cytotoxicity activities were higher than 17.08 µg/mL, indicating low toxicity. These findings suggest that silver oxide nanoparticles derived from *Ericaria amentacea* seaweed have potential applications in the treatment of leishmaniasis. Further research is needed to elucidate the mechanisms of action and assess the in vivo efficacy of these nanoparticles. Moreover, comprehensive toxicity studies are necessary before considering their clinical use in leishmaniasis treatment.

Keywords: brown seaweed; *Ericaria amentacea*; extraction; silver oxide nanoparticles; synthesis; characterization; anti-leishmanial activity; cytotoxicity test

1. Introduction

Leishmaniasis is a parasitic disease which is categorized as a neglected tropical disease (NTD) [1]. It is estimated that there are between 700,000 and 1 million new cases of Leishmaniasis each year [2]. The transmission of the disease occurs through approximately 90 species of sandflies, which can transmit the *Leishmania* parasites. These parasites consist of more than 20 species and contribute to an annual death toll of 20,000 to 30,000 [3]. Currently, there is no specific therapeutic treatment available for leishmaniasis. It is a

widespread disease that causes between 20,000 and 30,000 deaths each year, making it a major health problem in endemic areas. Due to the inefficacy of current medications, the improvement of leishmaniasis treatment via the administration of drugs poses a significant challenge [4,5].

Currently, the treatment of leishmaniasis relies on first-line drugs such as sodium stibogluconate (commercially known as pentostam) and meglumine antimoniate (commercially known as glucantime), along with alternative options (second-line drugs) such as pentamidine isothionate (commercially known as pentamidine), amphotericin B (Fungizone or ambisome), miltefosine, and paromomycin sulfate (Aminosidine) [6,7]. However, the use of paromomycin sulfate is not widely practiced in several countries due to health regulations, and it does not exhibit effectiveness when administered orally. Even when these medications are used in combination, their effectiveness falls short of achieving optimal results. The antimonial drugs (glucantime, pentostam, and pentamidine) were developed over 70 years ago and continue to be used in the treatment of leishmaniasis [8]. Some of these drugs have proven to be ineffective due to parasite resistance, and this has been compounded by limited development in this class of medications. These substances carry significant side effects, including renal failure, acute pancreatitis, myalgia, teratogenicity, peripheral neuropathy, hepatotoxicity, and cardiotoxicity (manifesting as cardiac arrhythmia). Furthermore, the treatment duration is often extended. In addition to their potential side effects, some of these medications can be expensive and may not always produce the desired outcomes due to parasite resistance [9]. Moreover, certain patients may face barriers when accessing healthcare systems, and individuals with renal, hepatic, or cardiac insufficiency, as well as those with tuberculosis, are unable to use these medications [10].

Natural products are either extracts or secondary metabolites found in the roots, stems, leaves, fruits, seeds, vegetables, and other specific parts of plants [11–13]. They exhibit a wide range of structural diversity that enables them to mediate interactions between plants and their environment. Numerous metabolites have been noted in the literature for their antiparasitic activity, particularly against leishmaniasis [14]. Specifically, marine organisms have been studied as a significant source of biologically active secondary metabolites. However, only a limited number of studies have evaluated the leishmanicidal activity of seaweed extracts. Brown seaweed of the genus *Cystoseira* (Cystoseiraceae) is widespread in tropical and subtropical regions and is well-known as a rich source of unique, structurally diverse, and biologically active diterpenes of mixed biogenesis (meroditerpenoids). Despite the numerous chemical studies available for the *Cystoseira* genus, only a few reports have described the potential anti-leishmanial effects of its crude extracts, and no information has been found regarding the compounds responsible for their inhibitory effects on *Leishmania* parasites [15,16].

In contrast, recent advancements in nanomedicine and nanotechnologies have opened up new possibilities for utilizing medicinal plants and chemical drugs [17]. These technologies involve incorporating these substances into carrier materials and manipulating them at a nanoscale level. This enables targeted delivery to specific host cells in various body regions, enhancing their effectiveness and reducing potential side effects [18]. This approach preserves or enhances the valuable pharmacological properties of these active products. Additionally, nanotechnology has the potential to improve existing standard treatments for diseases, including leishmaniasis, by increasing their bioavailability, reducing costs, and minimizing the toxicity and undesirable side effects associated with these active products [19,20].

To date, numerous studies have highlighted the remarkable biological activities of certain nanoparticles [21]. Among them, silver ions and silver nanoparticles have been widely recognized for their potent antimicrobial properties, particularly against *Leishmania* parasites [22]. Nanoparticle-based products, including those enriched with natural extracts, have emerged as highly effective compound-delivery systems, showcasing their potential in various applications. These nanoparticles facilitate the targeted delivery of therapeutic

compounds, attesting to their efficacy and offering promising solutions in the field. Thus, an appropriate process for the preparation of nanometallic extracts could enhance the efficacy of leishmanicidal activities. This advancement paves the way for innovative approaches to the development of more targeted and effective therapies against *Leishmania* parasites, which is crucial considering the prevalence of this disease in various regions worldwide. It is essential to focus these research efforts to better understand the mechanisms of action of nanoparticles and optimize their potential use in the treatment of parasitic diseases, thereby contributing to the advancement of medical therapies [23–25]. In this study, we synthesized four (4) silver oxide nanoparticles coated with four extracts from the *Ericaria amentacea* seaweed (Ea-AgNPs-A, Ea-AgNPs-B, Ea-AgNPs-C, and Ea-AgNPs-D) and characterized them using various techniques including transmission electron microscopy (TEM), UV spectrophotometry, X-ray diffraction (XRD), thermal gravimetric analysis (TGA), and Fourier transform infrared spectroscopy (FTIR). Furthermore, we investigated their *in vitro* antileishmanial activity against the three strains *Leishmania infantum*, *Leishmania tropica*, and *Leishmania major*. Additionally, we conducted a further study to assess their cytotoxic activities using a brine shrimp test.

2. Materials and Methods

2.1. Experimental Procedure

2.1.1. Chemical Reagents

Except for the algal biomass used in this study, all chemicals utilized were of analytical grade and were procured from Merck (Darmstadt, Germany) and ACROS (Geel, Belgium).

2.1.2. Preparation of Seaweed Extracts

After seaweed was harvested from the Gulf of Tadjourah (Djibouti) (11°47′09.3″ N, 42°52′40.7″ E) during low tide, it underwent a series of processing steps. Initially, the harvested seaweed was carefully washed with water to eliminate impurities. It was then allowed to naturally dry at room temperature in a shaded area for one day. Subsequently, the seaweed was further dried in an oven set at 40 °C for one week. Once the drying process was completed, the resulting biomass was finely ground into a powdered form. The subsequent step involved extracting the desired compounds from the seaweed using the soxhlet extraction method. This entailed the sequential use of solvents with increasing polarity: hexane (A), ether (B), chloroform (C), and methanol (D). After each extraction, the solvents were evaporated to obtain the desired extracts. The color and yield of each extract were determined and recorded for future reference. To ensure long-term stability and preservation, the extracts were stored in specifically designated brown bottles and kept in freezers at −80 °C until they were ready for subsequent use.

2.1.3. Phenolic Chemical Profiles of the Extracts

The chemical profiles of phenols are expressed by determining the total content of phenols, flavonoids, and tannins following the methods established by Elbouny et al. (2022) [26], Borah et al. (2022) [27], and Al-Dalahmeh et al. (2022) [28], respectively, with minor modifications.

The Folin–Ciocalteu method was used to quantify the total phenols. Essentially, 500 μL of 10% Folin–Ciocalteu reagent was mixed with an equal volume of 1 mg mL^{-1} extract in methanol in a 10 mL volumetric flask. The mixture was allowed to stand for 5 min, and then 1 mL of 7.5% (*w/v*) Na_2CO_3 was added. The volume was made up with distilled water, and the homogenized solution was incubated in the dark at room temperature for 2 h. The absorbance of the solution was read at 760 nm in a UV/Vis spectrophotometer. The blank consisted of methanol and all the other reagents except the extract. The total phenol content was obtained from the gallic acid standard curve at 2–10 $\mu\text{g mL}^{-1}$. The result was expressed in milligrams of gallic acid equivalents per gram of dry extract (mg GAE g^{-1}).

To estimate the total flavonoids, an analysis mixture containing 500 μL of 1 mg mL^{-1} extract in methanol, 500 μL of 60% glacial acetic acid, 2 mL of 20% pyridine in ethanol, and

1 mL of 5% aluminum chloride (methanol solution) was added to a 10 mL volumetric flask. The volume was made up with 80% methanol, and then the mixture was homogenized and incubated at room temperature for 30 min. The absorbance was then recorded at 420 nm. Methanol and all the other reagents except the extract were used as the blank. The flavonoid content was obtained using the quercetin standard curve at 2–10 $\mu\text{g mL}^{-1}$. The result was expressed in milligrams of quercetin equivalents per gram of dry extract (mg QE g^{-1}).

For the quantification of the tannin, a mixture of about 500 mg of casein, 500 μL of 2 mg mL^{-1} extract in methanol, and 5 mL of distilled water was prepared in a 25 mL Erlenmeyer flask. The mixture was then stirred at 600 rpm using a magnetic stirrer for 2 h (the time needed for tannin complexation with the total protein). Subsequently, the extract was filtered through Whatman 113 filter paper into a 10 mL volumetric flask, and the volume was adjusted with distilled water. An aliquot of 500 μL of this solution was then transferred to a 10 mL volumetric flask and processed using the Folin–Ciocalteu method described above for the determination of the total phenols. The difference in absorbance before and after casein precipitation was used for the calculations. The total tannin content was estimated using the tannic acid standard curve at 2–10 $\mu\text{g mL}^{-1}$ and expressed in milligrams of tannic acid equivalents per gram of dry extract (mg TAE g^{-1}).

2.1.4. Synthesis of Nanoparticles Using Seaweed Extracts

A solution containing 1.5288 g of AgNO_3 , corresponding to a concentration of 0.1 M, was prepared by dissolving the AgNO_3 in 90 mL of demineralized water. Following this, 10 mL of extracts A, B, C, and D were gradually added to the solution. Upon introducing the extracts, the initially colorless solution underwent a noticeable change, developing a brownish-black hue. This alteration signified the creation of silver oxide nanoparticles using extracts derived from *Ericaria amentacea* seaweed. The resultant mixture was continuously stirred and heated at a temperature of 70 ± 5 °C for a duration of 5 h. After the reaction, the mixture was allowed to cool to room temperature. For purification, the black-brown precipitate was washed thrice with ethanol and then subjected to centrifugation at 10,000 rpm for 20 min. Subsequently, the precipitate was dried overnight in a hot air oven at 100 ± 5 °C. The synthesized silver oxide nanoparticles, Ea-AgNPs-A, Ea-AgNPs-B, Ea-AgNPs-C, and Ea-AgNPs-D, obtained from extracts A, B, C, and D, respectively, were then transformed into fine powder and stored for subsequent analysis.

2.2. Analytical Instruments for Characterization

The nanoparticles were characterized using the following methods and equipment, following standard protocols:

- (i) UV-VIS spectrophotometer: a Shimadzu UV-1601, manufactured by Shimadzu Corporation in Tokyo, Japan, was employed to perform the spectrophotometric measurements.
- (ii) Transmission electron microscopy: a Philips JOEL TEM (New York, NY, USA) was utilized for this purpose.
- (iii) X-ray diffraction: a Bruker D8 Advance diffractometer with $\text{Cu K}\alpha$ radiation (wavelength: 1.54 Å), manufactured by Bruker Corporation in Billerica, MA, USA, was utilized to conduct the XRD analysis.
- (iv) Thermal gravimetry analysis: a thermal analyzer, specifically the DTG-60H system manufactured by Shimadzu in Kyoto, Japan, was used to perform the thermal gravimetry analysis. The analysis involved heating the samples in a temperature range of 0 to 700 °C at a rate of 10 °C/min.
- (v) Fourier transform infrared spectra: The FTIR spectra were obtained using a spectrophotometer known as the BRUKER VERTEX 70, manufactured by Bruker Corporation in Billerica, MA, USA. The spectra were collected within the range of 4000–400 cm^{-1} with a resolution of 4 cm^{-1} .

- (vi) Zeta potential analysis: the zeta potentials of each nanoparticle were measured using a Zetasizer model 3000HS, Malvern Instrument Ltd., Malvern, UK.

2.3. Biological Activities

2.3.1. Antileishmanial Tests

The MTT method employed in this study followed the steps outlined by Ainane et al. (2018) [16]. This colorimetric assay was used to assess the antileishmanial activity of the nanoparticles against promastigote forms of *Leishmania*. The principle of the test is based on the enzymatic reduction of the tetrazolium salt MTT (3-(4,5-dimethylthiazol-2-yl)-2,5-diphenyltetrazolium bromide) to formazan. During this process, viable cells containing mitochondrial succinate dehydrogenase actively reduce the tetrazolium ring of MTT, resulting in the formation of formazan. Formazan is a colored product, typically dark violet in color, that is insoluble in water. The intensity of this coloration is directly proportional to the number of viable cells present during the assay and their metabolic activity.

For the antileishmanial evaluations, cultures of promastigotes from three strains (*Leishmania infantum*, *Leishmania tropica*, and *Leishmania major*) were used. The promastigotes were maintained at 25 °C by subculturing every five days in RPMI 1640 medium without phenol red, buffered with 25 mM NaHCO₃ (pH ~ 7), and supplemented with 20% fetal bovine serum. The parasites were initially incubated in culture flasks at a concentration of 5 × 10⁵ parasites/mL. The parasite count was determined using a Malassez counter, and then the parasites were seeded into 96-well ELISA plates at a concentration of 2 × 10⁵ parasites/well in 90 µL of RPMI medium. The test products were prepared by dissolving them in 5% DMSO to achieve final concentrations of 20, 30, 40, and 50 µg/mL. As a solvent control, 100 µL of parasite culture mixed with 10 µL of DMSO was added to the wells in triplicate, resulting in an additional volume of 10 µL. After 72 h of incubation at 25 °C, 10 µL of MTT solution (5 mg/mL) was added to each well, and the plates were incubated again. Following a 2 h incubation at room temperature and an additional 3 h incubation at 37 °C, a violet color developed. Subsequently, the plates were centrifuged at 2500 rpm for 3 min, and 200 µL of DMSO was added to each well. The absorbance of each well was measured at 492 nm using an ELISA spectrophotometer (Thermo Scientific, Multiskan 60, Waltham, MA, USA).

The 50% inhibition concentration (IC 50) value was determined via linear interpolation on curves plotting the percentage of viability against the logarithm of the tested concentration. It should be noted that the percentage of viability was calculated using the following equation:

$$\%Viability = \frac{ABS_{Control} - ABS_{Sample}}{ABS_{Control}} \times 100$$

2.3.2. Cytotoxicity Tests

The cytotoxicity evaluation, commonly known as the brine shrimp test, employed in this study followed the methodology outlined by Bennamara and Abourriche (2020) [29]. This test assesses the toxic activity of the tested products by observing their impact on the larvae of saltwater shrimps (*Artemia salina*). Furthermore, it enables the determining of the lethal dose affecting 50% of the population (LD 50), facilitating comparisons of the tested products' toxicity with that of reference substances. The samples to be evaluated were dissolved in a 2% DMSO solution, yielding concentrations of 20, 40, 60, and 100 µg/mL. Subsequently, predetermined volumes of the prepared solution were introduced into tubes containing *Artemia salina* larvae. The tubes were then placed in a chamber at room temperature, and the outcomes were examined after 24 h by counting under a binocular microscope. In instances where the control group had deceased larvae, the mortality percentage was adjusted using the following formula:

$$\%Mortality = \frac{NDLP}{NDLC} \times 100$$

where % Mortality is the mortality percentage, NDLP is the number of dead larvae in the presence of the tested product, and NDLT is the number of dead larvae in the presence of the control (solvent).

2.4. Statistical Analysis

The statistical analyses were conducted using EXCEL and XLSTAT software (version 2020.1.3).

Group comparisons were performed using one-way ANOVA, while differences in numerical results were assessed using the Spearman correlation method. A significance level of $p < 0.05$ was considered statistically significant. To ensure accuracy and reliability, all experiments were conducted in triplicate.

The box plot was generated after evaluating the data series using the Dixon test, with a significance threshold of 5%, enabling the exclusion of outliers.

Principal component analysis (PCA) is a mathematical tool used in biological tests to explore the correlations between multiple parameters. Its purpose is to provide a comprehensive understanding of the relationships between the activity and the tested products.

2.5. Ethics Approval

All biological experimental and research procedures in the present work were conducted in accordance with the ethical guidelines and regulations set forth by the Superior School of Technology of Khenifra (EST-Khenifra) Committee at the University of Sultan My Slimane in Morocco. The study protocol received approval from the ethics committee under the ID 2023-0523-0002.

3. Results

Following the collection and drying of the *Ericaria amentacea* seaweed, four extracted products labeled A, B, C, and D were obtained through a series of successive extractions. One kilogram of the biomass was subjected to extraction using solvents with different polarity: hexane, ether, chloroform, and methanol. The resulting extracts were assessed for their color and yield in relation to the initial quantity of dried seaweed. Detailed information regarding the obtained products is provided in Table 1.

Table 1. The parameters of various extracts obtained from *Ericaria amentacea* seaweed.

| Extract | Color | Yield (%) |
|---------|--------------|-----------|
| A | Yellow-green | 3.84 |
| B | Green | 0.95 |
| C | Dark green | 1.33 |
| D | Green-black | 9.27 |

The quantification of the phenolic compounds, flavonoids, and tannins in each extract was conducted utilizing the calibration curves of the gallic acid ($y = 0.041x + 0.174$; $R^2 = 0.999$), quercetin ($y = 0.052x - 0.012$; $R^2 = 0.999$), and tannic acid ($y = 0.045x + 0.270$; $R^2 = 0.999$). The corresponding data are exhibited in Table 2. Analysis of variance (ANOVA) was employed to compare the means; any means not sharing a sequential designation were considered notably divergent ($p < 0.05$).

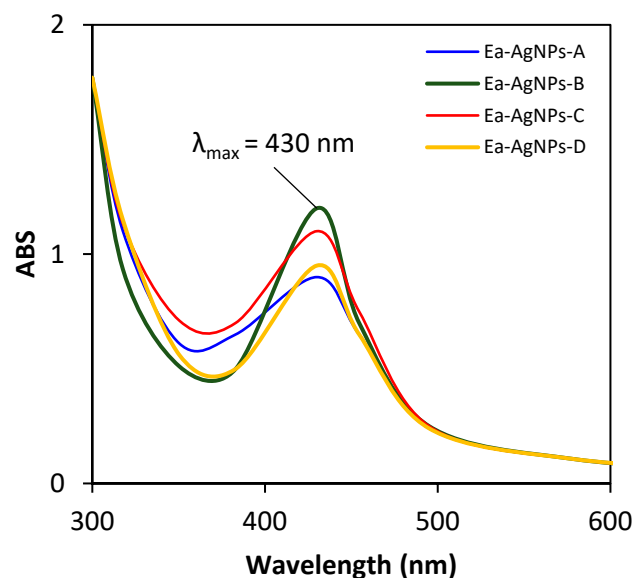
Table 2. The chemical profiles of phenols of extracts obtained from the algae *Ericaria amentacea*.

| Extract | A | B | C | D |
|---|----------------------------|----------------------------|----------------------------|----------------------------|
| Total phenols (mg GAE g ⁻¹) | 5.974 ± 0.194 ^a | 6.078 ± 0.212 ^a | 5.231 ± 0.190 ^b | 4.664 ± 0.183 ^c |
| Total flavonoids (mg QE g ⁻¹) | 0.611 ± 0.132 ^a | 0.885 ± 0.141 ^b | 0.602 ± 0.133 ^a | 0.458 ± 0.125 ^c |
| Total tannins (mg TAE g ⁻¹) | 0.050 ± 0.015 ^a | 0.057 ± 0.013 ^a | 0.048 ± 0.008 ^b | 0.037 ± 0.007 ^b |

Different letters in the same row indicate significant differences according to Tukey's test ($p < 0.05$).

The synthesis of the silver oxide nanoparticles was first confirmed through a noticeable color change. The original colorless AgNO₃ solution developed a brownish-black hue, indicating the successful formation of silver oxide nanoparticles when incorporating extracts A, B, C, and D. The compounds present in these extracts played a crucial role in capping and stabilizing the synthesized silver oxide nanoparticles, resulting in the formation of Ea-AgNPs-A, Ea-AgNPs-B, Ea-AgNPs-C, and Ea-AgNPs-D.

Figure 1 shows the UV-visible spectra of the silver oxide nanoparticles synthesized using the environmentally friendly method. The spectra reveal that the nanoparticles exhibited a maximum absorbance value at 430 nm. Furthermore, variations in absorbance were observed during the synthesis of different nanoparticles using different extracts of the *Ericaria amentacea* seaweed. It can be noted that ABS₄₃₀ (Ea-AgNPs-B) > ABS₄₃₀ (Ea-AgNPs-C) > ABS₄₃₀ (Ea-AgNPs-D) > ABS₄₃₀ (Ea-AgNPs-A), indicating that the compounds present in the ether extract exhibited a higher reactivity compared to those in the chloroform extract, followed by those in the methanol extract, and finally those in the hexane extract.

**Figure 1.** UV-visible spectra of the synthesized Ea-AgNPs.

The morphologies and sizes of the nanoparticles synthesized under light radiation were examined using TEM. Figure 2 illustrates representative TEM micrographs of the four synthesized nanoparticles, clearly demonstrating their spherical morphologies. The size distribution histogram obtained from the TEM scans illustrates their effective dispersion and fairly consistent sizes; the size of an average particle ranged from 15 nm to 45 nm. This measurement was obtained through the digital analysis of TEM images containing a minimum of 100 particles (Figure 3). Notably, the nanoparticles synthesized from the ether extract Ea-AgNPs-B appeared to be smaller than those synthesized from the chloroform extract Ea-AgNPs-C, methanol extract Ea-AgNPs-D, and hexane extract Ea-AgNPs-A.

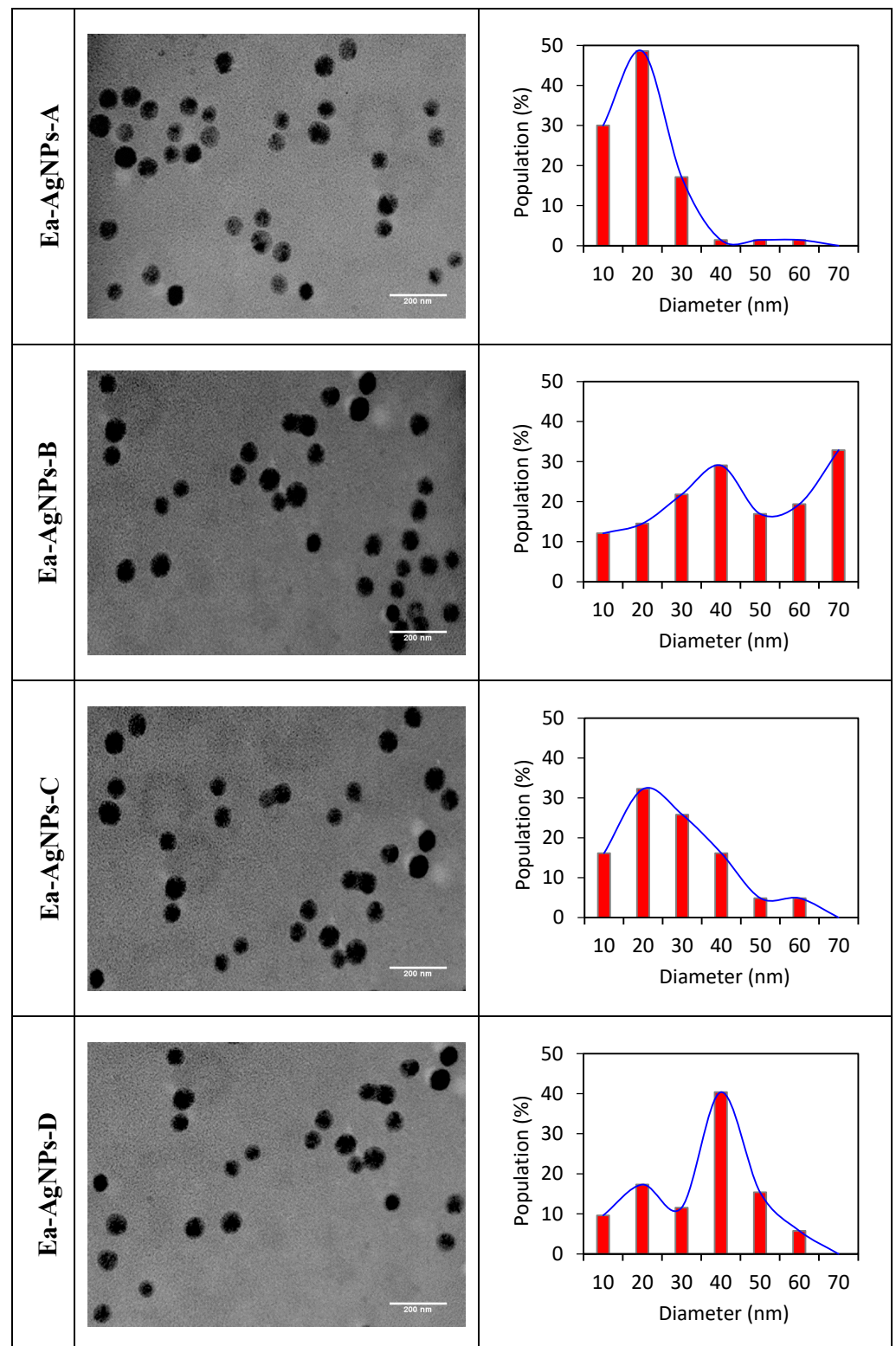


Figure 2. TEM images and corresponding particle size distribution histograms of the synthesized Ea-AgNPs.

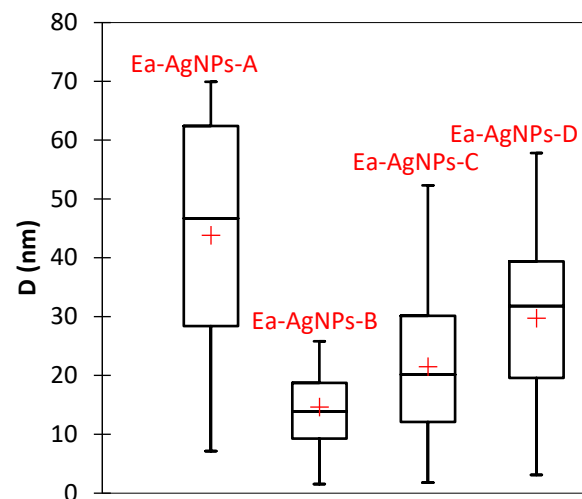


Figure 3. Box plot of particle sizes of the synthesized Ea-AgNPs.

Figure 4 displays the XRD patterns of the four silver oxide nanoparticles synthesized using the environmentally friendly method: Ea-AgNPs-A, Ea-AgNPs-B, Ea-AgNPs-C, and Ea-AgNPs-D. The patterns exhibit strong, intense, and sharp peaks at 2θ values of 32.17, 37.31, 53.80, 64.08, 67.29, and 79.55. The observed peaks in the XRD patterns correspond to the crystallographic planes (111), (200), (220), (311), (222), and (400). These XRD patterns indicate that the synthesized nanoparticles possess a face-centered cubic system with lattice parameters of $a = b = c = 4.816$ and $\alpha = \beta = \gamma = 90^\circ$. The presence of a high-intensity peak at the (111) plane suggests that the nanoparticles exhibit a preferred growth orientation in that direction. Furthermore, this peak indicates the highly crystalline nature of the synthesized nanoparticles [30–32].

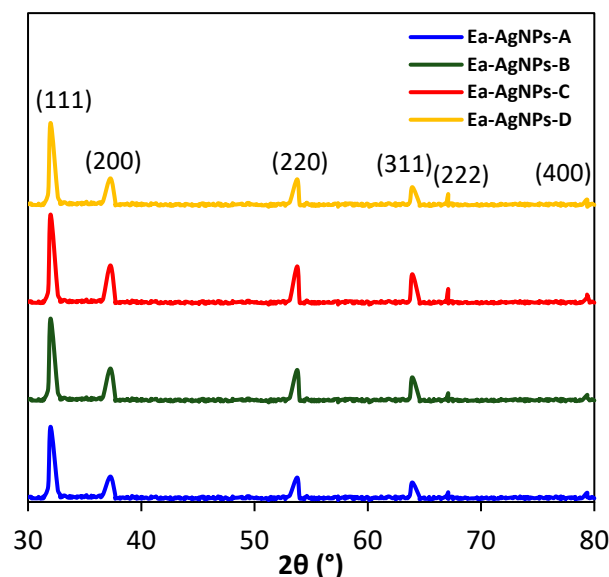


Figure 4. XRD patterns of the four synthesized Ea-AgNPs. (The labeled peaks correspond to the characteristic diffraction peaks of elemental AgO).

Figure 5 presents the thermogravimetric analysis (TGA) plots of the synthesized silver oxide nanoparticles Ea-AgNPs-A, Ea-AgNPs-B, Ea-AgNPs-C, and Ea-AgNPs-D. These plots exhibit similar curves and depict three significant weight losses across the entire temperature range.

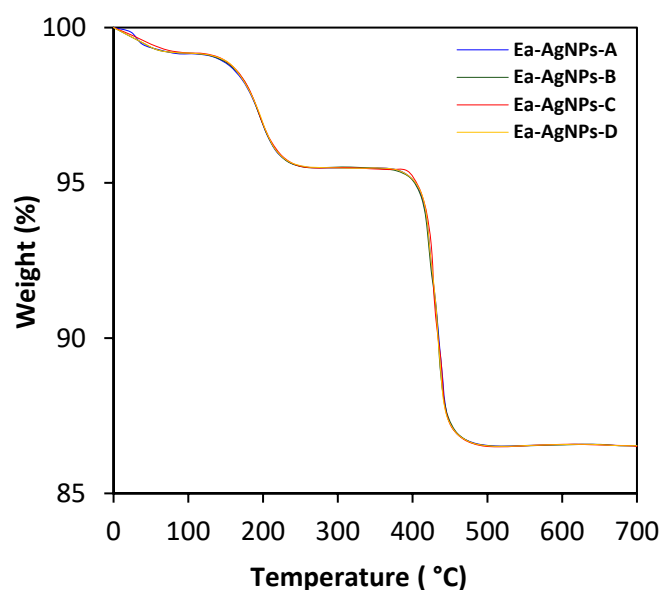
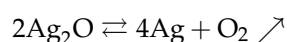


Figure 5. TGA curves of the synthesized Ea-AgNPs.

- The 1st weight loss, accounting for less than 1% of the total weight, occurs between 50 and 100 °C. This weight loss is attributed to the decomposition of organic compounds present on the surface of the nanoparticles.
- The 2nd weight loss, accounting for approximately 3.5%, takes place between 120 and 245 °C. It corresponds to the decomposition of AgO, leading to the formation of Ag₂O and the release of O₂ gas [33]. This reaction can be represented as:



- The 3rd weight loss, accounting for approximately 8%, occurs between 350 and 500 °C. It is associated with the decomposition of Ag₂O into Ag [34]. The reaction can be described as:



Overall, these TGA results provide insights into the thermal decomposition behavior of the synthesized silver oxide nanoparticles. They shed light on the transformations and reactions taking place within the nanoparticles in different temperature ranges.

To identify the functional groups involved in the synthesis of the silver nanoparticles, a FTIR analysis was performed. The control spectra of extracts A, B, C, and D exhibited multiple peaks, indicating the complex nature of their chemical composition. The intensities of the bands in different regions of the spectra of both the extracts and their corresponding silver oxide nanoparticles were analyzed and are presented in Figure 6. Generally, there was a slight shift observed in the nanoparticle peaks compared to the corresponding extracts, particularly in the regions around 2350, 1645, 1200, and 1050 cm⁻¹. The peak at around 2350 cm⁻¹ can be attributed to N-H stretching or C=O stretching vibrations [35]. Three peaks located at approximately 1645, 1200, and 1050 cm⁻¹ may correspond to the stretching vibrations of the C-O-H, OH, and C=O bonds present in polyphenols or carboxyl compounds [36–38]. These peaks suggest the involvement of these polyphenols in the reduction process during nanoparticle synthesis. Another significant observation was the well-defined peak observed in the spectra of all four nanoparticles—Ea-AgNPs-A, Ea-AgNPs-B, Ea-AgNPs-C, and Ea-AgNPs-D—at around 520 cm⁻¹, indicating the formation of silver oxide (AgO) [39].

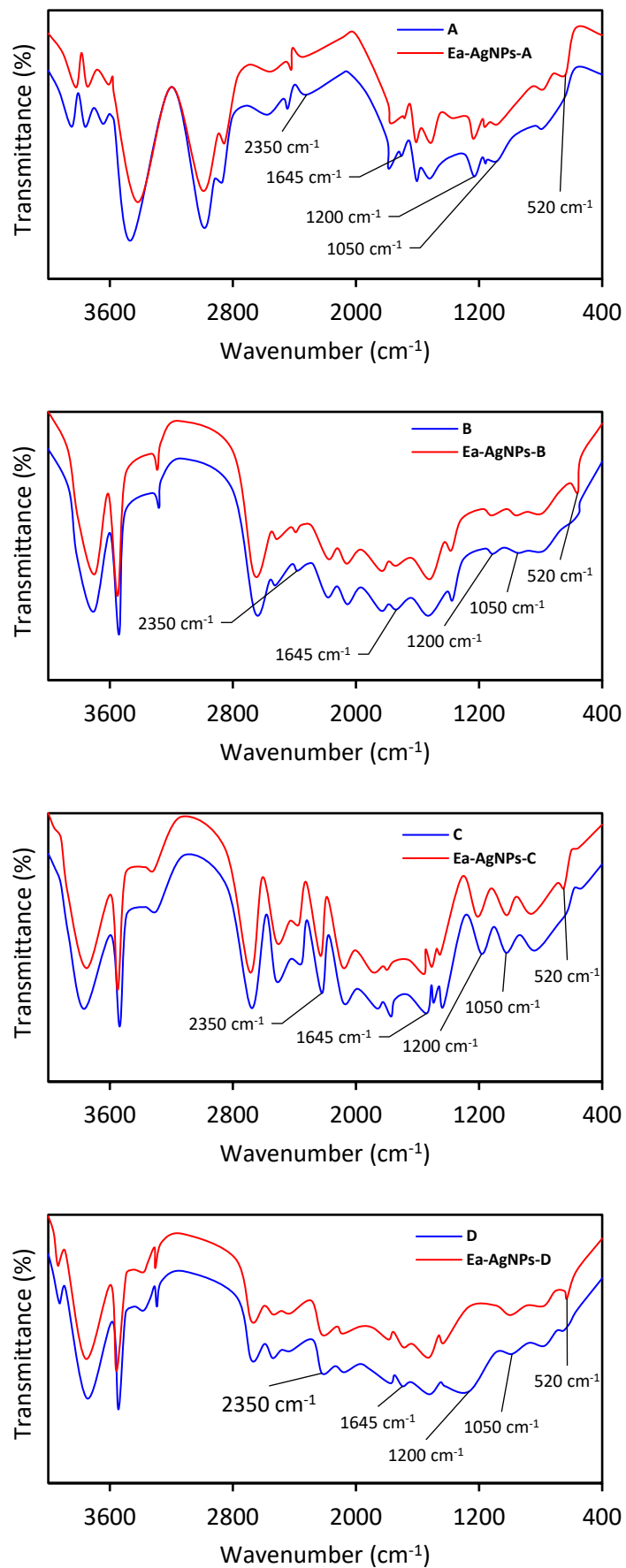


Figure 6. FTIR analysis of the synthesized Ea-AgNPs.

The zeta potential analysis provided a crucial parameter for determining the stability of the nanoparticle suspensions. For a physically stable nanoparticle suspension to be stabilized solely by electrostatic repulsion, a zeta potential of ± 30 mV is required as a minimum. The results of the analysis of the Zeta potential of the synthesized silver oxide nanoparticles were as follows: -45.1 ± 1.6 mV for Ea-AgNPs-A; -44.3 ± 1.5 mV for Ea-AgNPs-B; -45.8 ± 1.6 mV for Ea-AgNPs-C; and -46.0 ± 1.8 mV for Ea-AgNPs-D (Figure 7). These negative Zeta potential values indicate that the silver nanoparticles in each of the samples are negatively charged. In this case, higher values in terms of absolute magnitude indicate greater dispersion stability, suggesting stronger repulsion between particles, which prevents their aggregation. According to the means produced by the ANOVA test, the nanoparticle samples show no statistical difference at 5%, indicating a similar dispersion stability for all four samples.

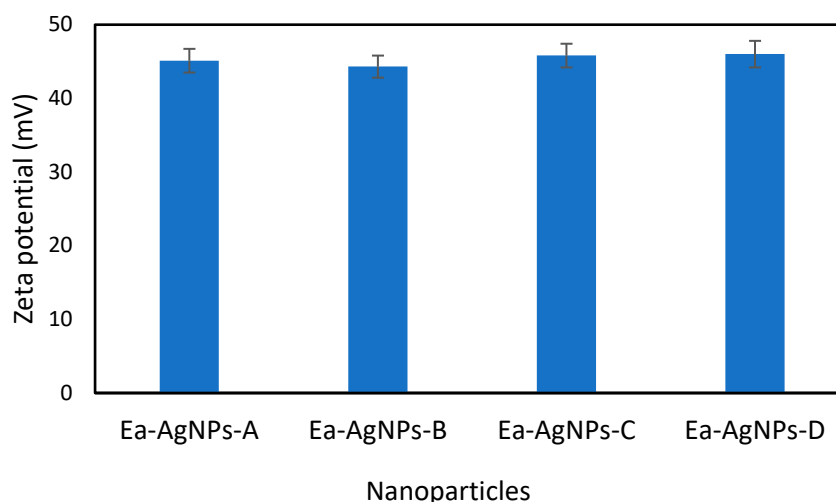


Figure 7. Zeta potential of the synthesized Ea-AgNPs.

Table 3 presents the inhibitory effects of the *Ericaria amentacea* extract variants A, B, C, and D, as well as those of their corresponding nanoparticles Ea-AgNPs-A, Ea-AgNPs-B, Ea-AgNPs-C, and Ea-AgNPs-D, against the strains *L. infantum*, *L. tropica*, and *L. major*. The table also includes the results of cytotoxicity tests against *Artemia salina*, thus presenting the values of the active ingredients for both biological tests. The results conclusively show that silver oxide-based nanoparticles demonstrate remarkable efficacy against the examined extracts in vitro, with a decrease in IC 50 values from the range of 42.08–105.21 $\mu\text{g}/\text{mL}$ to 27.16–38.18 $\mu\text{g}/\text{mL}$. However, the cell toxicity data reveal a substantial change in LD 50, indicating a potentially toxic aspect.

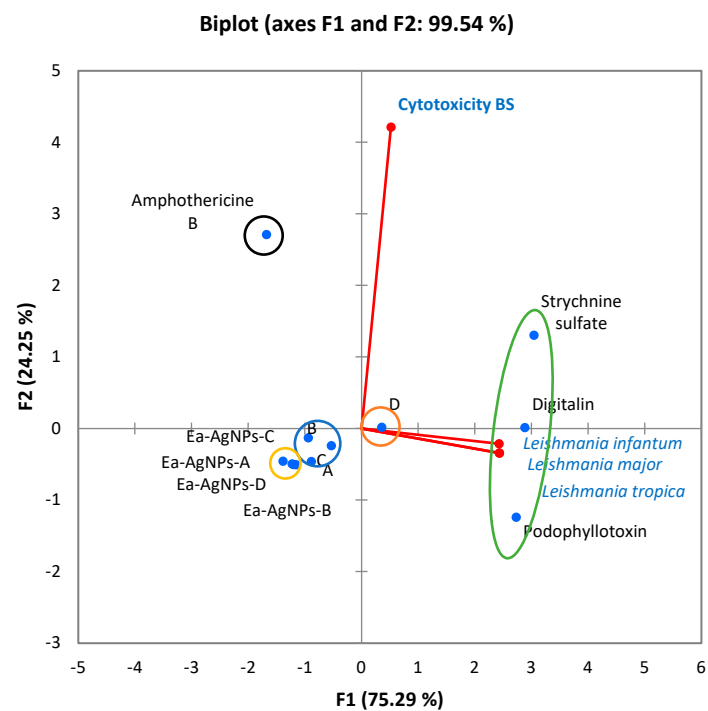
In general, the silver oxide nanoparticles exhibited anti-leishmanial properties against the three strains *L. infantum*, *L. tropica*, and *L. major*, with nonsignificant differences ($\alpha \leq 5\%$).

In order to provide a comprehensive explanation of the results, a principal component analysis was conducted in conjunction with the biological evaluations to examine the aforementioned correlations. The biplot in Figure 8 displays the results of the principal component analysis of the parameters, namely the 50% inhibition concentration of antileishmanial activity (IC 50) and the 50% lethal dose of cytotoxicity activity (LD 50). For the analysis, the most relevant axes—F1 and F2, which accounted for 75.29% and 24.25% of the information, respectively—were selected. Together, these axes explained 99.54% of the total inertia, indicating that a substantial amount of information was explained by each axis.

Table 3. IC 50 ($\mu\text{g/mL}$) values of the antileishmanian activities and LD 50 ($\mu\text{g/mL}$) values of the cytotoxicities of extracts obtained from *Ericaria amentacea* seaweed and their synthesized nanoparticles.

| Product | <i>L. infantum</i> | <i>L. tropica</i> | <i>L. major</i> | ANOVA | | Cytotoxicity BS |
|--------------------|-------------------------------|-------------------------------|--------------------------------|---------|--------------------|----------------------------|
| | IC 50 ($\mu\text{g/mL}$) | | | F-Ratio | p-Value | LD 50 ($\mu\text{g/mL}$) |
| A | 48.77 \pm 2.14 | 50.45 \pm 3.08 | 46.39 \pm 2.05 | 0.63 | 0.52 | 21.80 \pm 3.05 |
| B | 42.14 \pm 1.87 ^a | 42.08 \pm 1.82 ^a | 49.86 \pm 3.77 ^b | 214.22 | <0.05 [*] | 40.46 \pm 4.18 |
| C | 66.11 \pm 2.52 ^a | 56.41 \pm 3.14 ^b | 62.74 \pm 1.90 ^c | 174.92 | <0.05 [*] | 37.05 \pm 3.33 |
| D | 90.52 \pm 3.01 ^a | 94.78 \pm 3.14 ^b | 105.21 \pm 5.24 ^c | 154.07 | <0.05 [*] | 58.24 \pm 4.46 |
| Ea-AgNPs-A | 33.12 \pm 2.54 | 35.74 \pm 2.88 | 35.75 \pm 2.94 | 0.52 | 0.61 | 17.41 \pm 2.82 |
| Ea-AgNPs-B | 27.41 \pm 2.32 | 27.16 \pm 2.34 | 29.53 \pm 2.78 | 0.71 | 0.48 | 18.42 \pm 2.87 |
| Ea-AgNPs-C | 35.87 \pm 2.12 | 36.25 \pm 2.55 | 35.74 \pm 2.26 | 0.48 | 0.75 | 17.08 \pm 2.01 |
| Ea-AgNPs-D | 37.7 \pm 2.87 | 38.18 \pm 2.63 | 37.49 \pm 2.71 | 0.68 | 0.57 | 17.25 \pm 2.50 |
| Amphotericine B | 0.24 \pm 0.05 | 0.26 \pm 0.05 | 0.23 \pm 0.05 | 0.33 | 0.81 | - |
| Podophyllotoxin | - | - | - | - | - | 2.45 \pm 0.41 |
| Digitalin | - | - | - | - | - | 76.23 \pm 5.17 |
| Strychnine sulfate | - | - | - | - | - | 152.14 \pm 6.99 |

The use of different letters in the same row indicates that there are significant differences between the groups, as determined using Tukey's test with a significance level of $p < 0.05$. * Values are significant at $p < 0.05$. (-): not tested.

**Figure 8.** Biplot of the correlations between the products tested and the antileishmanian and cytotoxicity activities.

Based on the grouping analysis, the tested products can be categorized into five classes:

- The first class comprises only amphotericin, which shows promise as a therapeutic alternative in leishmaniasis treatment.
- The second class consists of cytotoxic activity control substances, namely podophyllotoxin, digitalin, and strychnine sulphate.
- The third class includes the four nanoparticles Ea-AgNPs-A, Ea-AgNPs-B, Ea-AgNPs-C, and Ea-AgNPs-D.
- The fourth class comprises extracts A, B, and C.
- The fifth class includes extract D.

These findings indicate that all of the tested products, except extract D, exhibited remarkable and similar antileishmanial activities against the three strains *L. infantum*, *L. tropica*, and *L. major*. Extract D showed moderate activity.

Regarding toxicity, when compared to other products, all of the extracts and synthesized nanoparticles demonstrated lower toxicity than podophyllotoxin and higher toxicity than digitalin and strychnine sulfate.

4. Discussion

Nanomedicine has opened innovative prospects by effectively harnessing natural resources and medicinal agents through their transformation into nanoscale particles. This conversion enables the precise targeting of host cells in various bodily regions while preserving or enhancing the essential pharmacological characteristics of the particles [40–44]. The dynamic realm of nanotechnology encompasses the green synthesis of these nanoparticles, offering ecologically responsible approaches to the design of nanoscale materials with unique properties. Green synthesis strategies can be adjusted according to the physicochemical properties one wishes to obtain [45].

Simultaneously, leishmaniasis, as a form of microbial infection and parasitic disease leading to cutaneous or visceral ailments, can result in debilitating consequences, even mortality, without treatment. These pathologies are caused by diverse parasites of the *Leishmania* genus which are transmitted through sandfly bites. For the past several decades, amphotericin B has prevailed as the recommended standard treatment and primary chemotherapeutic option for all forms of leishmaniasis. Nevertheless, severe side effects, high costs, pronounced toxicity, and parasite resistance to traditional chemical compounds have spurred researchers' efforts towards creating more economically viable and safer innovative therapies against leishmaniasis [46–49]. In this context, in-depth research which aims to discover new drugs with ingenious delivery systems and distinct mechanisms of action remains imperative.

Seaweeds, which are repositories of bioactive phytoconstituents, also stand out because they can enhance the leishmanicidal properties of steroids, alkaloids, triterpenoids, and even meroditerpenoids. This approach aligns with the vision of nanomedicine, which holds the potential to improve the conventional recommended treatments for various conditions, including leishmaniasis. Nanomedicine paves the way to increased drug bioavailability, reduced costs, and the mitigation of the toxicity and undesirable side effects associated with prescribed medications. Recent advancements have identified such potential in numerous secondary metabolites from seaweed [50,51].

Ongoing studies highlight the potential benefits of silver nanoparticles encapsulated with natural substance extracts in leishmaniasis management through biological trials. Inherent challenges in the use of drug treatments motivate the quest for new therapeutic approaches. These approaches aim to be more affordable, less toxic, and more innovative [37–40]. In this context, thorough investigations aiming to identify beneficial therapeutic agents equipped with ingenious delivery systems and distinct mechanisms of action are crucial for more effective leishmaniasis management.

In this study, after the synthesis of the silver nanoparticles using the extracts obtained from *Ericaria amentacea* via the soxhlet method, a physicochemical characterization was performed to determine the structural and morphological properties of the nanomaterials. The main techniques used for the characterization of silver nanoparticles were UV spectrophotometry (UV), transmission electron microscopy (TEM), X-ray diffraction (XRD), thermal gravimetry analysis (TGA), Fourier-transform infrared spectroscopy (FTIR), and zeta potential. UV-VIS spectroscopy confirmed the characteristic color changes observed during the synthesis of the silver nanoparticles, with a maximum wavelength recorded at $\lambda_{\text{max}} = 430$ nm. Determining the size distribution of the AgNPs was crucial, and this was accomplished using transmission electron microscopy (TEM), which provided several physical characteristics based on their shape and size. X-ray diffraction (XRD) was employed to identify the crystalline nature of the nanoparticles, and the presence of three

diffraction peaks—(111), (200), and (220)—indicated that the synthesized nanoparticles possessed a face-centered cubic system. Additionally, a gravimetric analysis indicated the presence of organic matter and silver oxide in the synthesized nanoparticles, as observed in the thermogram. These aforementioned findings were further supported by a Fourier-transform infrared spectroscopy (FTIR) analysis, which identified the functional groups used in the synthesis of the silver nanoparticles, where the bands of polyphenols were reduced during synthesis (1645, 1200, and 1050 cm^{-1}), and that a characteristic band appeared in the nanoparticles at 520 cm^{-1} . Finally, the zeta potential analysis demonstrated that the silver oxide nanoparticles showcased comparable dispersion steadiness, even though there were minor discrepancies in their negative charge measurements.

The antileishmanial activity of the silver nanoparticles synthesized from the seaweed *Ericaria amentacea* has shown promising results compared to other extracts, though this has been accompanied by a slight increase in cytotoxicity. The precise mechanisms of the antimicrobial effects of the nanoparticles are not yet fully understood. However, according to the literature, it is hypothesized that nanoparticles can induce catalytic oxidation, bind to proteins and cellular components, and release ions, all of which contributes to their antimicrobial activity [52,53]. Some nanoparticles can generate reactive oxygen species (ROS) when exposed to ultraviolet (UV) light, enabling them to eliminate microorganisms. Macrophages naturally produce high levels of ROS to eliminate microbial agents such as viruses, fungi, and parasites [54–56]. Leishmania parasites have developed enzymatic mechanisms to inhibit ROS production in macrophages, allowing them to survive as host cells. However, ROS-inducing nanoparticles can overcome this inhibition and eliminate Leishmania parasites [57–59]. The mechanisms of action by which nanoparticles produce their antileishmanial effects can be attributed to several factors. On one hand, their small size and large specific surface area facilitate better penetration of parasitic cells, thereby enhancing their effectiveness [56]. On the other hand, nanoparticles can generate reactive oxygen species, such as free radicals, which are toxic to parasites, causing damage to their cellular structures and metabolic processes [60]. Moreover, nanoparticles can disrupt the cell membranes of parasites, altering their integrity and leading to their demise. It is worth noting that the use of nanoparticles has the potential to reduce required drug dosages, consequently minimizing undesirable side effects in patients [61]. Furthermore, nanoparticles can be tailored to specifically target parasitic cells, further increasing their effectiveness and reducing harm to healthy host cells [62].

Overall, the results underscore the potential of utilizing nanoparticles for drug delivery to reduce the parasitic burden, offering a promising avenue for managing leishmaniasis. Given the challenges posed by this parasitic disease, the imperative development of novel therapeutic strategies becomes evident. Silver oxide nanoparticles derived from green synthesis using *Ericaria amentacea* algae holds promise in this regard. However, within the medical domain, the use of silver oxide nanoparticles carries potential risks that warrant consideration. While their antimicrobial properties generate enthusiasm for treating infections, potential adverse effects come to the forefront. Among these potential dangers are cellular cytotoxicity, which can impact both healthy cells and targeted microorganisms and have adverse effects on the balance of the endogenous microbial flora [63,64]. Additionally, the emerging threat of microbial resistance to silver nanoparticles could potentially restrict their long-term effectiveness. Nevertheless, despite their encouraging potential, it remains pivotal to continue research for a more comprehensive understanding of the mechanisms of action of nanoparticles within the context of leishmaniasis. Thorough assessments of long-term safety and clinical efficacy are imperative. While in vitro studies constitute a critical initial step in determining their potential, comprehensive clinical investigations will be necessary to ascertain their true utility in leishmaniasis treatment. Ultimately, the integration of nanoparticles into the medical field presents a promising advancement that could revolutionize our approach to managing parasitic diseases and other pathologies.

5. Conclusions

Industrialization and the rapid growth in the global population have spurred an increasing demand for innovative solutions in the medical and pharmaceutical sectors. The necessity for environmentally friendly products and effective materials for biomedical applications has driven research in this field. This study aimed to address these challenges by conducting the eco-friendly synthesis of silver oxide nanoparticles using extracts from *Ericaria amentacea* seaweed. This green synthesis approach aligns with the goals of a sustainable and environmentally friendly economy. The bioactive properties of these nanoparticles were assessed through antileishmanial and cytotoxicity analyses, confirming their effectiveness. These nanoparticles show promising potential as antileishmanial agents, meeting the growing requirements of the medical and pharmaceutical industries in an eco-friendly and sustainable manner.

Author Contributions: Conceptualization, F.M.A.-L.; methodology, I.H.A. and M.L.; software, A.A. (Ayoub Ainane), B.H.K., M.L. and A.A. (Abdelmjid Abourriche); validation, F.M.A.-L.; formal analysis, F.M.A.-L., A.A. (Ayoub Ainane), M.L. and A.A. (Abdelmjid Abourriche); investigation, T.A.; data curation, I.H.A., J.M. and T.A.; writing—review and editing, F.M.A.-L., A.A. (Ayoub Ainane) and T.A.; visualization, T.A.; supervision, F.M.A.-L.; project administration, F.M.A.-L.; funding acquisition, F.M.A.-L. All authors have read and agreed to the published version of the manuscript.

Funding: This research received no external funding.

Data Availability Statement: Data are contained within the article.

Conflicts of Interest: The authors declare no conflict of interest.

References

1. Mengarda, A.C.; Iles, B.; Longo, J.P.F.; de Moraes, J. Recent approaches in nanocarrier-based therapies for neglected tropical diseases. *Wiley Interdiscip. Rev. Nanomed. Nanobiotechnol.* **2023**, *15*, e1852. [[CrossRef](#)] [[PubMed](#)]
2. Ornellas-Garcia, U.; Cuervo, P.; Ribeiro-Gomes, F.L. Malaria and leishmaniasis: Updates on co-infection. *Front. Immunol.* **2023**, *14*, 1122411. [[CrossRef](#)]
3. Sampaio, R.N.R. Pharmacotherapy in leishmaniasis: Old, new treatments, their impacts and expert opinion. *Expert Opin. Pharmacother.* **2023**, *24*, 153–158. [[CrossRef](#)] [[PubMed](#)]
4. Pal, R.; Teli, G.; Matada, G.S.P. The role of natural anti-parasitic guided development of synthetic drugs for leishmaniasis. *Eur. J. Med. Chem.* **2023**, *258*, 115609. [[CrossRef](#)] [[PubMed](#)]
5. Chastonay, A.H.; Chastonay, O.J. Housing risk factors of four tropical neglected diseases: A brief review of the recent literature. *Trop. Med. Infect. Dis.* **2022**, *7*, 143. [[CrossRef](#)]
6. Majumder, N.; Banerjee, A.; Saha, S. A review on new natural and synthetic anti-leishmanial chemotherapeutic agents and current perspective of treatment approaches. *Acta Trop.* **2023**, *240*, 106846. [[CrossRef](#)]
7. García-Estrada, C.; Pérez-Pertejo, Y.; Domínguez-Asenjo, B.; Holanda, V.N.; Murugesan, S.; Martínez-Valladares, M.; Reguera, R.M. Further Investigations of Nitroheterocyclic Compounds as Potential Antikinetoplastid Drug Candidates. *Biomolecules* **2023**, *13*, 637. [[CrossRef](#)]
8. Registre, C.; Soares, R.D.; Rubio, K.T.; Santos, O.D.; Carneiro, S.P. A Systematic Review of Drug-Carrying Nanosystems Used in the Treatment of Leishmaniasis. *ACS Infect. Dis.* **2023**, *9*, 423–449. [[CrossRef](#)]
9. Imran, M.; Khan, S.A.; Abida; Alshrari, A.S.; EltahirMudawi, M.M.; Alshammari, M.K.; Alshammari, N.A. Small molecules as kinetoplastid specific proteasome inhibitors for Leishmaniasis: A patent review from 1998 to 2021. *Expert Opin. Ther. Pat.* **2022**, *32*, 591–604. [[CrossRef](#)]
10. Daher, E.D.F.; da Silva Junior, G.B.; Trivedi, M.; Fayad, T.; Srisawat, N.; Nair, S.; Jha, V. Kidney complications of parasitic diseases. *Nat. Rev. Nephrol.* **2022**, *18*, 396–406. [[CrossRef](#)]
11. Abdoul-Latif, F.M.; Elmi, A.; Merito, A.; Nour, M.; Risler, A.; Ainane, A.; Ainane, T. Essential oils of *Tagetes minuta* and *Lavandulacoronopifolia* from Djibouti: Chemical composition, antibacterial activity and cytotoxic activity against various human cancer cell lines. *Int. J. Plant Biol.* **2022**, *13*, 315–329. [[CrossRef](#)]
12. Abdoul-Latif, F.M.; Ainane, A.; Merito, A.; Ainane, T. Chemical composition and biological activities of essential oils from Djibouti. *J. Anal. Sci. Appl. Biotechnol.* **2022**, *4*, 1–9.
13. Ainane, A.; Cherroud, S.; El Kouali, M.; Abba, E.H.; Ainane, T. Chemical compositions, insecticidal and antimicrobial activities of two moroccan essential oils of *Citrus limonum* and *Syzygium aromaticum*. *Pharmacologyonline* **2020**, *30*, 190–199.
14. de Castro Levatti, E.V.; Costa-Silva, T.A.; Morais, T.R.; Fernandes, J.P.S.; Lago, J.H.G.; Tempone, A.G. Lethal action of Licarin A derivatives in *Leishmania (L.) infantum*: Imbalance of calcium and bioenergetic metabolism. *Biochimie* **2023**, *208*, 141–150. [[CrossRef](#)] [[PubMed](#)]

15. Ainane, T.; Abourriche, A.; Kabbaj, M.; Elkouali, M.; Bennamara, A.; Charrouf, M.; Lemrani, M. Biological activities of extracts from seaweed *Cystoseira tamariscifolia*: Antibacterial activity, antileishmanial activity and cytotoxicity. *J. Chem. Pharm. Res.* **2014**, *6*, 607–611.
16. Ainane, T.; Abourriche, A.; Bennamara, A.; Talbi, M.; Lemrani, M. Activité anti-leishmanienne des extraits d'une algue brune *Bifurcariabifurcata* de la côte atlantique du Maroc. *Phytothérapie* **2018**, *16*, 68–73. [[CrossRef](#)]
17. Assolini, J.P.; Carloto, A.C.M.; da Silva Bortoleti, B.T.; Gonçalves, M.D.; Pellissier, F.T.; Feuser, P.E.; Pavanelli, W.R. Nanomedicine in leishmaniasis: A promising tool for diagnosis, treatment and prevention of disease—An update overview. *Eur. J. Pharmacol.* **2022**, *923*, 174934. [[CrossRef](#)]
18. Tuon, F.F.; Dantas, L.R.; de Souza, R.M.; Ribeiro, V.S.T.; Amato, V.S. Liposomal drug delivery systems for the treatment of leishmaniasis. *Parasitol. Res.* **2022**, *121*, 3073–3082. [[CrossRef](#)]
19. Jia, Y.; Jiang, Y.; He, Y.; Zhang, W.; Zou, J.; Magar, K.T.; Boucetta, H.; Teng, C.; He, W. Approved Nanomedicine against Diseases. *Pharmaceutics* **2023**, *15*, 774. [[CrossRef](#)]
20. Abpeikar, Z.; Safaei, M.; Alizadeh, A.A.; Goodarzi, A.; Hatam, G. The novel treatments based on tissue engineering, cell therapy and nanotechnology for cutaneous leishmaniasis. *Int. J. Pharm.* **2023**, *633*, 122615. [[CrossRef](#)]
21. Gopu, B.; Kour, P.; Pandian, R.; Singh, K. Insights into the drug screening approaches in leishmaniasis. *Int. Immunopharmacol.* **2023**, *114*, 109591. [[CrossRef](#)] [[PubMed](#)]
22. Krishnaraj, C.; Kaliannagounder, V.K.; Rajan, R.; Ramesh, T.; Kim, C.S.; Park, C.H.; Yun, S.I. Silver nanoparticles decorated reduced graphene oxide: Eco-friendly synthesis, characterization, biological activities and embryo toxicity studies. *Environ. Res.* **2022**, *210*, 112864. [[CrossRef](#)] [[PubMed](#)]
23. de Santana, N.S.; de Oliveira de Siqueira, L.B.; do Nascimento, T.; Santos-Oliveira, R.; dos Santos Matos, A.P.; Ricci-Júnior, E. Nanoparticles for the treatment of visceral leishmaniasis. *J. Nanopart. Res.* **2023**, *25*, 24. [[CrossRef](#)]
24. González, M.A.C.; Gonçalves, A.A.M.; Ottino, J.; Leite, J.C.; Resende, L.A.; Melo-Júnior, O.A.; Giunchetti, R.C. Vaccination with formulation of nanoparticles loaded with *Leishmania amazonensis* antigens confers protection against experimental visceral Leishmaniasis in hamster. *Vaccines* **2023**, *11*, 111. [[CrossRef](#)]
25. Khan, M.M.; Zaidi, S.S.; Siyal, F.J.; Khan, S.U.; Ishrat, G.; Batool, S.; Din, F. Statistical optimization of co-loaded rifampicin and pentamidine polymeric nanoparticles for the treatment of cutaneous leishmaniasis. *J. Drug Deliv. Sci. Technol.* **2023**, *79*, 104005. [[CrossRef](#)]
26. Elbouny, H.; Ouahzizi, B.; Bakali, A.H.; Sellam, K.; Chakib, A.L.E.M. Phytochemical study and antioxidant activity of two Moroccan Lamiaceae species: *Nepeta nepetella* subsp. *amethystina* and *Sideritis arborescens* Salzm. ex Benth. *J. Anal. Sci. Appl. Biotechnol.* **2022**, *4*, 15–21.
27. Borah, A.; Selvaraj, S.; Holla, S.R.; De, S. Extraction and characterization of total phenolic and flavonoid contents from bark of *Swietenia macrophylla* and their antimicrobial and antioxidant properties. *Arab. J. Chem.* **2022**, *15*, 104370. [[CrossRef](#)]
28. Al-Dalameh, Y.; Al-Bataineh, N.; Al-Balawi, S.S.; Lahham, J.N.; Al-Momani, I.F.; Al-Sheraideh, M.S.; Mayyas, A.S.; Abu Orabi, S.T.; Al-Qudah, M.A. LC-MS/MS screening, total phenolic, flavonoid and antioxidant contents of crude extracts from three asclepiadaceae species growing in Jordan. *Molecules* **2022**, *27*, 859. [[CrossRef](#)]
29. Bennamara, A.; Abourriche, A. Alkaloids 8-Hydroxyquinoline derivatives: Synthesis and biological activities. *J. Anal. Sci. Appl. Biotechnol.* **2020**, *2*, 57–62.
30. Maduraimuthu, V.; Ranishree, J.K.; Gopalakrishnan, R.M.; Ayyadurai, B.; Raja, R.; Heese, K. Antioxidant Activities of Photoinduced Photogenic Silver Nanoparticles and Their Potential Applications. *Antioxidants* **2023**, *12*, 1298. [[CrossRef](#)]
31. Gecer, E.N.; Erenler, R. Biogenic synthesis of silver nanoparticles using *Echium vulgare*: Characterisation, quantitative analysis of bioactive compounds, antioxidant activity and catalytic degradation. *J. Indian Chem. Soc.* **2023**, *100*, 101003. [[CrossRef](#)]
32. Sharma, A.; Sagar, A.; Rana, J.; Rani, R. Green synthesis of silver nanoparticles and its antibacterial activity using fungus *Talaromyces purpureogenus* isolated from *Taxus baccata* Linn. *Micro Nano Syst. Lett.* **2022**, *10*, 2. [[CrossRef](#)]
33. Kipke, A.; Hofmeister, H. Formation of silver nanoparticles in low-alkali borosilicate glass via silver oxide intermediates. *Mater. Chem. Phys.* **2008**, *111*, 254–259. [[CrossRef](#)]
34. Kayed, K. The optical properties of individual silver nanoparticles in Ag/Ag₂O composites synthesized by oxygen plasma treatment of silver thin films. *Plasmonics* **2020**, *15*, 1439–1449. [[CrossRef](#)]
35. Khammour, F.; Abdoul-Latif, F.M.; Ainane, A.; Mohamed, J.; Ainane, T. Eco-friendly adsorbent from waste of mint: Application for the removal of hexavalent chromium. *J. Chem.* **2021**, *2021*, 8848964. [[CrossRef](#)]
36. Espina, A.; Sanchez-Cortes, S.; Jurašeková, Z. Vibrational study (Raman, SERS, and IR) of plant gallnut polyphenols related to the fabrication of iron gall inks. *Molecules* **2022**, *27*, 279. [[CrossRef](#)]
37. Petrisor, G.; Motelica, L.; Ficai, D.; Trusca, R.D.; Surdu, V.A.; Voicu, G.; Oprea, C.; Ficai, A.; Andronesu, E. New mesoporous silica materials loaded with polyphenols: Caffeic acid, ferulic acid and p-coumaric acid as dietary supplements for oral administration. *Materials* **2022**, *15*, 7982. [[CrossRef](#)]
38. Saroha, V.; Khan, H.; Raghuvanshi, S.; Dutt, D. Development of polyvinyl alcohol-based antioxidant nanocomposite films with nanokaolin impregnated with polyphenols from pomegranate peel extract. *Food Packag. Shelf Life* **2022**, *32*, 100848. [[CrossRef](#)]
39. Allaka, G.; King, M.F.L.; Yepuri, V.; Narayana, R.L. Synthesis of silver oxide nanoparticles using gomutra mediation and their investigations on anti-oxidant property. *Mater. Today Proc.* **2023**. [[CrossRef](#)]
40. Haleem, A.; Javaid, M.; Singh, R.P.; Rab, S.; Suman, R. Applications of Nanotechnology in Medical field. *Glob. Health J.* **2023**, *3*, 5–11.

41. Sahu, T.; Ratre, Y.K.; Chauhan, S.; Bhaskar, L.V.K.S.; Nair, M.P.; Verma, H.K. Nanotechnology based drug delivery system: Current strategies and emerging therapeutic potential for medical science. *J. Drug Deliv. Sci. Technol.* **2021**, *63*, 102487. [[CrossRef](#)]
42. Modi, S.; Prajapati, R.; Inwati, G.K.; Deepa, N.; Tirth, V.; Yadav, V.K.; Yadav, K.K.; Islam, S.; Gupta, P.; Kim, D.-H.; et al. Recent trends in fascinating applications of nanotechnology in allied health sciences. *Crystals* **2021**, *12*, 39. [[CrossRef](#)]
43. Khan, A.U.; Khan, M.; Cho, M.H.; Khan, M.M. Selected nanotechnologies and nanostructures for drug delivery, nanomedicine and cure. *Bioprocess Biosyst. Eng.* **2020**, *43*, 1339–1357. [[CrossRef](#)] [[PubMed](#)]
44. Grodzinski, P.; Kircher, M.; Goldberg, M.; Gabizon, A. Integrating nanotechnology into cancer care. *ACS Nano*. **2019**, *13*, 7370–7376. [[CrossRef](#)]
45. Konvičková, Z.; Schröfel, A.; Kolenčík, M.; Dědková, K.; Peikertová, P.; Žídek, M.; Kratošová, G. Antimicrobial bionanocomposite—from precursors to the functional material in one simple step. *J. Nanopart.* **2016**, *18*, 368. [[CrossRef](#)]
46. Almeida, J.R.; Gomes, A.; Mendes, B.; Aguiar, L.; Ferreira, M.; Brioschi, M.B.C.; Duarte, D.; Nogueira, F.; Cortes, S.; Salazar-Valenzuela, D.; et al. Unlocking the potential of snake venom-based molecules against the malaria, Chagas disease, and leishmaniasis triad. *Int. J. Biol. Macromol.* **2023**, *242*, 124745. [[CrossRef](#)]
47. Kumi, R.O.; Oti, B.; Abo-Dya, N.E.; Alahmdi, M.I.; Soliman, M.E. Bridging the gap in Malaria Parasite Resistance, current interventions, and the Way Forward from in Silico Perspective: A review. *Molecules* **2022**, *27*, 7915. [[CrossRef](#)]
48. Martínez-Peinado, N.; Cortes-Serra, N.; Losada-Galvan, I.; Alonso-Vega, C.; Urbina, J.A.; Rodríguez, A.; VandeBerg, J.L.; Cortes-Serra, N.; Gascon, J.; Alonso-Padilla, J. Emerging agents for the treatment of Chagas disease: What is in the preclinical and clinical development pipeline? *Expert Opin. Investig. Drugs* **2020**, *29*, 947–959. [[CrossRef](#)]
49. Khetmalis, Y.M.; Shivani, M.; Murugesan, S.; Sekhar, K.V.G.C. Oxindole and its derivatives: A review on recent progress in biological activities. *Biomed. Pharmacother.* **2021**, *141*, 111842. [[CrossRef](#)]
50. Kuzminac, I.Z.; Savić, M.P.; Ajduković, J.; Nikolić, A.R. Steroid and triterpenoid compounds with antiparasitic properties. *Curr. Top. Med. Chem.* **2023**, *23*, 791–815.
51. Zhang, M.; Zhang, Q.; Zhang, Q.; Cui, X.; Zhu, L. Promising Antiparasitic Natural and Synthetic Products from Marine Invertebrates and Microorganisms. *Mar. Drugs* **2023**, *21*, 84. [[CrossRef](#)] [[PubMed](#)]
52. Gold, K.; Slay, B.; Knackstedt, M.; Gaharwar, A.K. Antimicrobial activity of metal and metal-oxide based nanoparticles. *Adv. Ther.* **2018**, *1*, 1700033. [[CrossRef](#)]
53. Wang, L.; Hu, C.; Shao, L. The antimicrobial activity of nanoparticles: Present situation and prospects for the future. *Int. J. Nanomed.* **2017**, *12*, 1227–1249. [[CrossRef](#)] [[PubMed](#)]
54. Zhang, Z.; Chen, H.; Wang, Y.; Zhang, N.; Trépout, S.; Tang, B.Z.; Gasser, G.; Li, M.H. Polymersomes with Red/Near-Infrared Emission and Reactive Oxygen Species Generation. *Macromol. Rapid Commun.* **2023**, *44*, 2200716. [[CrossRef](#)] [[PubMed](#)]
55. Sarkar, A.R.; Pal, S.; Sarkar, A.K.; Jana, N.R. Hemin-based cell therapy via nanoparticle-assisted uptake, intracellular reactive oxygen species generation and autophagy induction. *New J. Chem.* **2022**, *46*, 21746–21755. [[CrossRef](#)]
56. Wang, Y.; Pu, M.; Yan, J.; Zhang, J.; Wei, H.; Yu, L.; Yan, X.; He, Z. 1,2-Bis(2-aminophenoxy)ethane-N,N,N', N'-tetraacetic Acid Acetoxymethyl Ester Loaded Reactive Oxygen Species Responsive Hyaluronic Acid–Bilirubin Nanoparticles for Acute Kidney Injury Therapy via Alleviating Calcium Overload Mediated Endoplasmic Reticulum Stress. *ACS Nano* **2022**, *17*, 472–491.
57. Khan, T.A.; Mnasri, A.; Al Nasr, I.S.; Özdemir, I.; Gürbüz, N.; Hamdi, N.; Koko, W.S. Activity of benzimidazole derivatives and their N-heterocyclic carbene silver complexes against leishmania major promastigotes and amastigotes. *Biointerface Res. Appl. Chem.* **2022**, *13*, 132–133.
58. Martínez-Esquivias, F.; Guzmán-Flores, J.M.; Pérez-Larios, A.; González Silva, N.; Becerra-Ruiz, J.S. A review of the antimicrobial activity of selenium nanoparticles. *J. Nanosci. Nanotechnol.* **2021**, *21*, 5383–5398. [[CrossRef](#)]
59. Hoseinzadeh, E.; Makhdoumi, P.; Taha, P.; Hossini, H.; Stelling, J.; Amjad Kamal, M.; Md Ashraf, G. A review on nano-antimicrobials: Metal nanoparticles, methods and mechanisms. *Currentdrugmetabolism* **2017**, *18*, 120–128. [[CrossRef](#)]
60. Yan, L.; Gu, Z.; Zhao, Y. Chemical mechanisms of the toxicological properties of nanomaterials: Generation of intracellular reactive oxygen species. *Chem.–Asian J.* **2013**, *8*, 2342–2353. [[CrossRef](#)]
61. Konvičková, Z.; Holišová, V.; Kolenčík, M.; Niide, T.; Kratošová, G.; Umetsu, M.; Seidlerová, J. Phytosynthesis of colloidal Ag–AgCl nanoparticles mediated by *Tilia* sp. leachate, evaluation of their behaviour in liquid phase and catalytic properties. *Colloid Polym. Sci.* **2018**, *296*, 677–687. [[CrossRef](#)]
62. Unciti-Broceta, J.D.; Arias, J.L.; Maceira, J.; Soriano, M.; Ortiz-González, M.; Hernández-Quero, J.; Garcia-Salcedo, J.A. Specific cell targeting therapy bypasses drug resistance mechanisms in African trypanosomiasis. *PLoSpathogens* **2015**, *11*, e1004942. [[CrossRef](#)] [[PubMed](#)]
63. Das, S.; Langbang, L.; Haque, M.; Belwal, V.K.; Aguan, K.; Roy, A.S. Biocompatible silver nanoparticles: An investigation into their protein binding efficacies, anti-bacterial effects and cell cytotoxicity studies. *J. Pharm. Anal.* **2021**, *11*, 422–434. [[CrossRef](#)]
64. Holsing, J.J.; Gaikwad, J. Electrically modified lyophilic silver hydrosol inhibits bacterial growth in a dose-dependent manner in vitro and in vivo. *Bios* **2023**, *94*, 36–41. [[CrossRef](#)]

Disclaimer/Publisher’s Note: The statements, opinions and data contained in all publications are solely those of the individual author(s) and contributor(s) and not of MDPI and/or the editor(s). MDPI and/or the editor(s) disclaim responsibility for any injury to people or property resulting from any ideas, methods, instructions or products referred to in the content.